

# Slow Light and Signal Processing in Silicon Nano-waveguides

Yikai Su (1), Qiang Li (1), Fangfei Liu (1), Qingjiang Chang (1), Ziyang Zhang (2), and Min Qiu (2)

1: State Key Lab of Advanced Optical Communication Systems and Networks, Department of Electronic Engineering

Shanghai Jiao Tong University, 800 DongChuan Rd, Shanghai 200240, China, yikaisu@sjtu.edu.cn

2: Department of Microelectronics and Applied Physics, Royal Institute of Technology, Sweden

**Abstract**-We report various all-optical signal processing functions using silicon microring resonators with a 450×250-nm cross section. These demonstrations include slow-light delay of phase-modulated data and microwave photonic signal, wavelength conversion/multicasting, format conversions, and optical differentiation.

## I. INTRODUCTION

Silicon-on-insulator (SOI) structure offers an excellent platform for monolithic integration of photonic devices due to its high index contrast between the silicon core and the silica substrate, allowing strong confinement of light and enabling ultra-compact devices. Silicon ring resonators with high Q-values can be explored for all-optical signal processing functions to achieve compact device size, high date rate, and low power consumption.

In this paper, we firstly study the system performances of an on-chip slow-light device based on the silicon micro-ring resonator for different modulation formats, including return-to-zero (RZ), carrier-suppressed return-to-zero (CSRZ), return-to-zero duobinary (RZ-DB), and return-to-zero alternate-mark-inversion (RZ-AMI). On-chip optical delay line is attractive due to its potential applications in future optical interconnections and packet-switching systems for data buffering and synchronization. Furthermore, we demonstrate that the device can be used to delay microwave photonic signals. Conventionally, a practical implementation of arrays with thousands of elements is limited by the size and complexity of the phase-shifting elements. However, the use of miniaturized and integrated devices to perform this function is of much interest due to the advantages of low cost, compact size and on-chip integration.

We then demonstrate dense wavelength conversion based on free-carrier dispersion effect induced by non-linear absorption in a silicon micro-ring resonator. In the previous reports, the control (pump) and signal resonances are separated by at least one free spectrum range (FSR). For small-radius ring resonators in SOI, large FSRs usually limit the choices of wavelengths that can be converted. Mutual mode coupling due to sidewall gratings generates both propagating and counter-propagating modes. The grating and in turn the split-resonance separation can be tuned by varying the E-beam lithography scan size and exposure dose. The split modes enable more channels for conversions, thus increasing

the system capacity. We demonstrate high-speed wavelength conversion using the split modes at 1-Gb/s rate. In addition, we demonstrate wavelength multicasting in this mode-split microring resonator. Wavelength multicasting is a process where a single data packet is converted into packets at multiple wavelengths. Previous multicasting approaches mainly used discrete devices such as semiconductor optical amplifier (SOA) and highly nonlinear fiber. Simultaneous wavelength conversion to multiple channels in the silicon photonic devices has not been demonstrated. In our experiment, a 1.25-Gb/s non-return-to-zero (NRZ) data carried by a pump signal is simultaneously converted to two probes located at the two resonance splits spaced by ~0.32 nm.

By using the mode-split ring resonator, we also propose and experimentally demonstrate format conversion from NRZ to frequency shift keying (FSK) based on the free carrier dispersion effect induced selective filtering. The split mode can provide large and variable frequency deviation for the FSK signal. FSK format has received considerable attention in passive optical network (PON) applications which are an attractive solution to provide broadband access. In this paper, 1-Gb/s NRZ signal is successfully converted to FSK format with a frequency deviation of 40 GHz. We also perform 10-Gb/s format conversion from NRZ to AMI signal using the linear filtering effect, which is the highest rate in silicon microring resonator, to the best of our knowledge. AMI is a RZ-like format with phase inversions that improve the signal tolerance to nonlinear propagation effects.

Finally, we show that the microring resonator can be employed in analog applications. Optical temporal differentiator, which takes the time derivative of the complex optical field, would be useful in analog-digital conversion, pulse shaping, and optical processing of microwave signals. Several methods have been proposed based on long-period and phase-shifted fiber gratings, transversal filter structure, and Mach-Zehnder interferometer. However, most of these optical differentiators are discrete devices and exhibit a size of ~1 mm or larger. To the best of our knowledge, no experimental demonstration has been performed with ultra-compact, integrated, optical differentiator on chip. Here, we demonstrate an optical temporal differentiator based on a silicon microring resonator operating near the critical coupling region. This differentiator can process signals with

data rates up to 10G. The performance of the device is tested using signals with typical shapes such as square, Gaussian, and sinusoidal pulses.

## II. EXPERIMENTAL SETUP AND RESULTS

### A. Silicon Microring Device

The silicon microrings in our experiments are fabricated on SOI wafer with a 250-nm-thick silicon slab on top of a 3- $\mu\text{m}$  silica buffer layer [1]. The cross section of the silicon waveguides is  $450\times250$  nm with a mode area of about  $0.1\mu\text{m}^2$  for transverse-electric (TE) optical mode in such a high-index-contrast structure. The microrings are side coupled to the straight waveguides with an air gap of 120 nm. The radii of the rings range from 10  $\mu\text{m}$  to 40  $\mu\text{m}$ . The devices are fabricated by E-beam lithography followed by reactive ion etching. The surface roughness is reduced by oxidizing 20 $\text{\AA}$  of silicon surfaces using wet chemistry. A scanning electron microscope (SEM) photo of a 10- $\mu\text{m}$  radius silicon microring resonator is shown in Fig. 1. At each end of the straight silicon waveguide, gold grating is added to couple light near-vertically with the single mode fiber (SMF). There is an adiabatic taper between the grating coupler and a 150- $\mu\text{m}$ -long access straight waveguide. This vertical coupling method has advantages in terms of easy alignment and simple fabrication of the mode converter compared to other coupling methods. The measured fiber-to-fiber coupling loss is  $\sim 20$  dB.

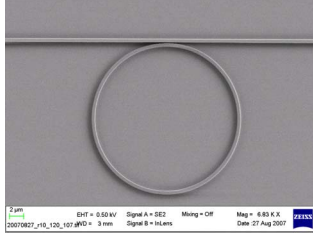


Fig. 1. SEM photo of a 10- $\mu\text{m}$  silicon microring.

### B. All-optical slow-light delay

The experimental setup is depicted in Fig. 2 [2]. A single drive Mach-Zehnder modulator (MZM) is driven by a 5-Gb/s pseudo-random bit sequence (PRBS) signal with a length of  $2^{15}-1$  to generate NRZ format. A second MZM, which acts as a pulse carver, is sinusoidally driven by a synchronized radio-frequency (RF) signal to produce CSRZ or RZ signals, respectively. The first single drive MZM is replaced by a dual-drive MZM when generating RZ-DB and RZ-AMI signals. The output data is boosted by an erbium-doped fiber amplifier (EDFA) and then filtered by a tunable band-pass filter (BPF) with a bandwidth of 1.6 nm. The signal power injected into the fiber is controlled below 0 dBm to avoid nonlinear effect. Four modulation formats are examined. The CSRZ format shows an optical phase flip between adjacent pulses. In RZ-DB, a  $\pi$ -phase shift occurs whenever there are odd number of 0-bits between two 1-bits; while for RZ-AMI the phase flips for each 1-bit, independent of the number of 0-bits in between. These four modulation formats show improved performances in high-speed optical systems

relative to the conventional NRZ signal. The RZ and CSRZ signals have been widely used in long-haul high-capacity wavelength division multiplexed (WDM) networks. RZ-AMI possesses better nonlinear performance through transmission, while RZ-DB shows narrow spectral width and thus enhanced tolerance to dispersion. Fig. 3 shows the eye diagrams for the 5-Gb/s RZ, CSRZ, RZ-DB and RZ-AMI signals when off-resonance and on-resonance, respectively. The delay is defined by comparing the peak points with maximal eye-openings. The maximum delays for the RZ, CSRZ, RZ-DB and RZ-AMI signals are 80 ps, 95 ps, 110 ps and 62 ps, respectively. These differences in group delay mainly result from spectral features of the formats. The eyes are open for the four eye diagrams when on resonance. The ripples appear before each ‘1’ bit, which were observed in the delayed CSRZ, RZ-DB and RZ-AMI signals. These ripples are related to the negative third-order dispersion on resonance. The ‘1’-level fluctuation in the delayed CSRZ, RZ-DB and RZ-AMI signals result from data pattern dependence.

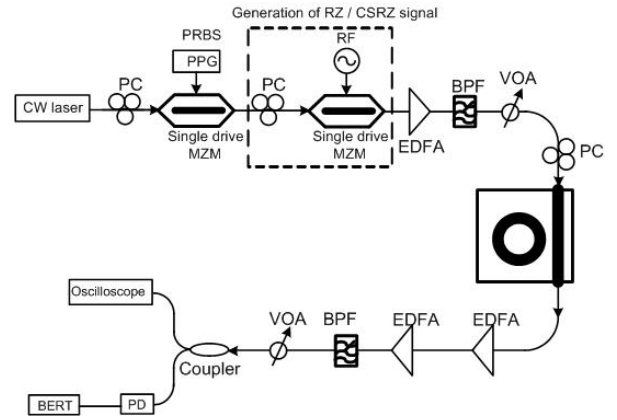


Fig. 2. Experimental setup for delay different formats.

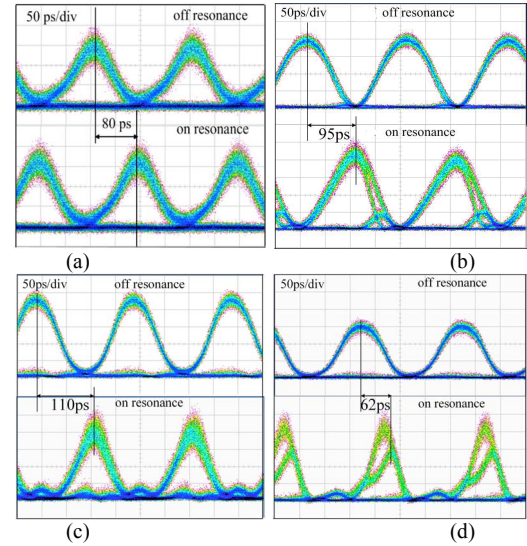


Fig. 3. Eye diagrams for the 5-Gb/s (a) RZ, (b) CSRZ, (c) RZ-DB, and (d) RZ-AMI signals when off resonance and on resonance, respectively.

### C. Microwave photonic phase shifter

A continuous wave (CW) signal from a tunable laser is fed into a single drive MZM, which is biased at the null and driven by a 10-GHz clock signal to produce a 20-GHz optical carrier suppression (OCS) signal. The pump light is amplified by a high power erbium doped fiber amplifier followed by an attenuator to adjust the pump power. Both the pump light and the probe signals are coupled through a 3-dB coupler to the microring resonator by a vertical coupling system. The output signal of the microring resonator is amplified using an EDFA and the probe signal is separated from the pump wave by a bandpass filter and sent to an oscilloscope to record the waveforms and measure the phase shift [3].

We firstly measure the dependence of the phase shift and the output power on the signal wavelength, as shown in Fig. 4. The maximum phase shift is -4.6 rad ( $\sim 260^\circ$ ) and the output power change is less than 2.2 dB, which mainly results from the loss of one sideband in the resonance region. We did not reach the desired maximum phase shift of  $2\pi$  rad since the 20-GHz spaced sidebands sit in the vicinity of the resonance and thus they did not experience the  $2\pi$  relative phase shift. For the maximum phase shift of  $\sim 4.6$  rad, the signal waveform still shows good quality, as shown in Fig. 5.

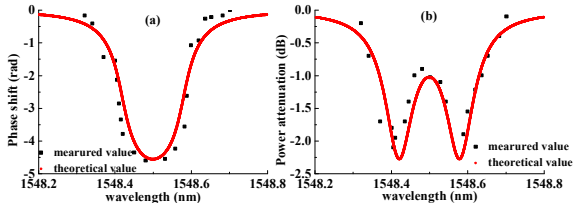


Fig. 4 The dependence of the phase shift and output power on signal wavelength.

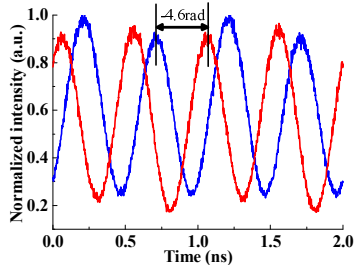


Fig. 5 The waveform of the 20G OCS signal when the maximum phase shift is 4.6 rad.

#### D. Wavelength conversion/multicasting

The sidewall gratings along the 10- $\mu\text{m}$ -radius ring give rise to the mode splitting effect [4] as shown in Fig. 6(a). The left resonance at 1552.534 nm has a full-width half-maximum bandwidth ( $\Delta\lambda_{\text{FWHM}}$ ) of 0.092 nm and the notch depth is 13.2 dB, while the right resonance is at 1552.947 nm with  $\Delta\lambda_{\text{FWHM}}$  of 0.071 nm and a notch depth of 12.4 dB. The signal wavelength  $\lambda_1$  is close to the left resonance for the non-inverted case and  $\lambda_2$  around the left resonance for the inverted case. The pump power is 14.3 dBm and the signal power is 6 dBm at the input of the fiber. Both non-inverted and inverted waveforms at 1 Gb/s are provided in Fig. 6(b).

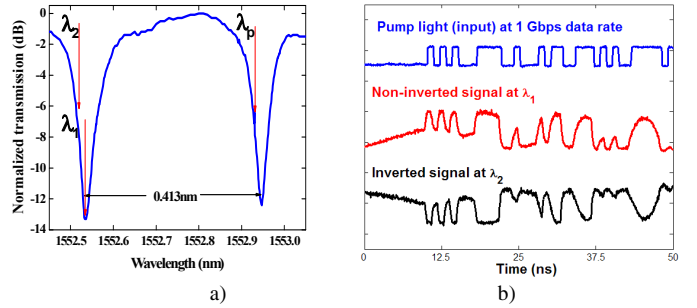


Fig. 6. (a) resonance spectrum, (b) converted signal waveforms.

We then experimentally demonstrate wavelength multicasting based on the free-carrier dispersion effect in the silicon mode-split microring resonator. Wavelength multicasting is a process where a single data packet is converted into packets at multiple wavelengths. In our experiment, a 1.25-Gb/s NRZ data carried by a pump signal is converted to two probes located at the two resonance splits spaced by  $\sim 0.32$  nm simultaneously. Two CW probe lights located at the vicinity of the two split resonances are combined using a 50:50 coupler and then amplified using an EDFA. The NRZ pump light is modulated using a MZM driven by a 1.25-Gb/s PRBS signal with a pattern length of  $2^7-1$ . The pump signal and two probes are combined using a 90:10 coupler so that the pump power is sufficiently high. The two converted probes are separated using a tunable bandpass filter with a 3-dB bandwidth of 0.3 nm. The pump power measured at the input fiber is  $\sim 18$  dBm and the one for the two probes is  $\sim 5$  dBm. The measured waveforms are shown in Fig. 7. Fig. 7(b) and (c) represent the non-inverted wavelength multicasting, in which the probes are placed at the right edge of the resonance; Fig. 7(d) and (e) show the case with the inversion of the '0' and '1' of the pump signal, in which the probes are placed at the left edge of the resonance. In both cases, there is little interference between the two channels.

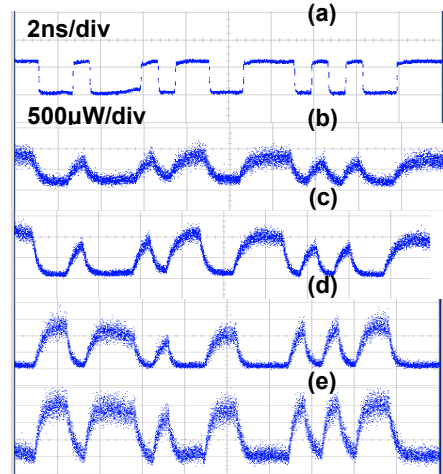


Fig. 7. Waveforms for (a) NRZ pump signal; converted probe signal at (b) left resonance split and (c) right resonance split; converted probe signal with inversion of '0' and '1' at (d) left resonance split and (e) right resonance split.

#### E. Format conversions

For the NRZ to FSK conversion, two CW probe lights are generated based on OCS modulation by driving a single drive MZM using a 20 GHz sinusoidal signal. The NRZ pump light is modulated using a MZM driven by a 1-Gb/s PRBS signal with a pattern length of  $2^7$ -1. The pump signal and the two probes are combined using a 3-dB coupler. The converted FSK signal is demodulated using a tunable bandpass filter with a 3-dB bandwidth of 0.3 nm.

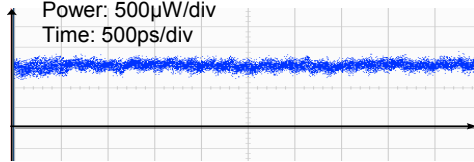


Fig. 8. Eye diagram of the converted FSK signal

The measured eye diagram of the converted FSK signal is shown in Fig. 8. The eye diagram of the converted FSK signal possesses almost constant envelope and the power difference of the two sidebands is less than 1 dB. Fig. 9 shows the demodulated FSK signals at two sidebands using a tunable band pass filter with a 3-dB bandwidth of 0.3 nm. The lower sideband carries the same information as the NRZ signal and the upper sideband carries the inverted information.

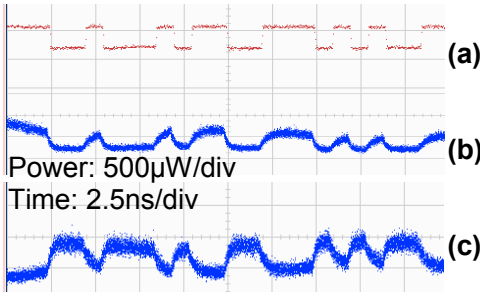


Fig. 9 Waveforms of (a) NRZ signal, demodulated FSK signal at the (b) upper sideband, (c) lower sideband.

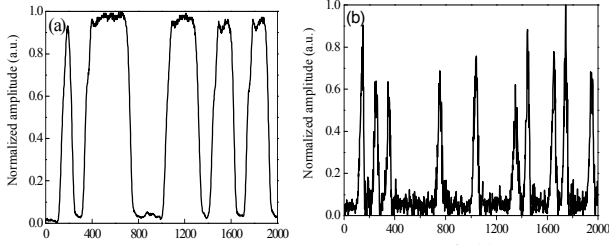


Fig. 10 (a) and (b) are waveforms of the input NRZ signal and the converted AMI signal, respectively.

NRZ to AMI conversion can be performed by using a high-Q ring resonator with a radius of 40  $\mu\text{m}$  as a narrow band filter, if the central component of the input NRZ signal can be well suppressed. Fig. 10(a) and (b) depict the waveforms of the input NRZ data and the converted AMI data, respectively. Sharp pulses of AMI data appear at both the rising and falling edges in “1” bits of NRZ data due to the effective suppression of the optical carrier and thus enhancement of the optical clock component in the notch filter transmission. The AMI

data has a pulse width of  $\sim 32$  ps and provides well-defined 10-GHz clock information.

#### F. Optical differentiation

Under the condition of critical coupling and the frequency detuning much less than the 3-dB bandwidth, the transfer function of a microring resonator can be approximated as  $T(\omega)=j(\omega-\omega_0)/r_0$ , where  $\omega_0$  is the resonance frequency and  $r_0$  is the energy decay rate related to the intrinsic loss. This equation is a typical function for a first-order temporal differentiator. Fig. 11 shows differentiation results of the 10G Gaussian, sinusoidal, and square pulses, respectively. The differentiation of a Gaussian-like pulse results in two symmetric pulses in intensity, and the two pulses are odd-symmetric in the optical field. The differentiation output of the sinusoidal-like pulses is nearly the same as the input pulses, while the differentiation of the square pulse generates impulses at the rising and falling edge.

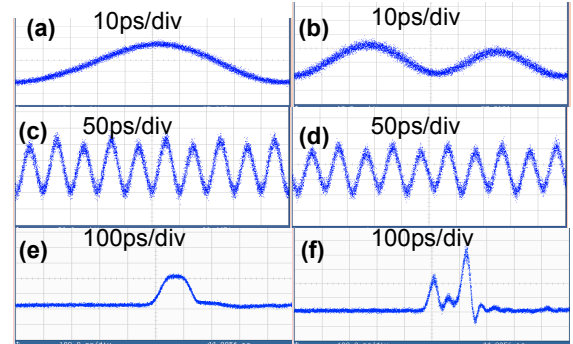


Fig. 11 Waveforms of (a), (b) Gaussian-like pulse; (c), (d) sinusoidal-like pulse; (e), (f) square pulse before and after differentiation.

#### IV. CONCLUSIONS

We demonstrate various optical signal processing functions using silicon microring resonators with a  $450 \times 250$ -nm cross section. These demonstrations include all-optical delay of 5-Gb/s RZ, CSRZ, RZ-AMI, RZ-DB, and 20-GHz photonic microwave signals; dense wavelength conversion; 2-channel wavelength multicasting; format conversions from NRZ to FSK and NRZ to AMI; and optical differentiation of analog signals.

#### ACKNOWLEDGMENT

This work was supported by the NSFC (60777040), Shanghai Rising Star Program Phase II (07QH14008), Swedish Foundation for Strategic Research (SSF), and the Swedish Research Council (VR).

#### REFERENCES

- [1] F. Liu, *et al.*, "Optically Tunable Delay Line in Silicon Microring Resonator Based on Thermal Nonlinear Effect," *IEEE JSTQE*, May/June, 2008
- [2] Qiang Li, *et al.*, "Performance of a Silicon-Microring Slow-Light Delay Line for Advanced Modulation Formats," in *Proc. OSA Slow and Fast Light Topic Meeting*, paper SMC5, 2008
- [3] Qiang Li, *et al.*, "Optically Tuneable Microwave Photonic Phase Shifter Based on Silicon Microring Resonator," in *Proc. ECOC P.2.12*, 2008
- [4] Ziyang Zhang, *et al.*, "Wavelength Conversion in a Silicon Mode-Split Micro-Ring Resonator with 1G Data Rate," in *Proc. CLEO/QELS*, paper CTuT2, 2008